Multiple Conformations of RGDW and DRGDW: A Theoretical Study and Comparison with NMR Results

Roland H. Stote,*,† Annick P. Dejaegere,†,‡ Jean-Francois Lefèvre,‡,§ and Martin Karplus*,†,||

Laboratoire de Chimie Biophysique, ISIS−CNRS ESA7006, Université Louis Pasteur, 4 rue Blaise Pascal, 67000 Strasbourg, France, Ecole Supérieure de Biotechnologie de Strasbourg, Groupe de RMN, Boulevarde Sébastien Brant, 67400 Illkirch-Graffenstaden, France, and Department of Chemistry, Harvard University, Cambridge, Massachusetts 02138

Received: June 25, 1999

The utility of molecular dynamics simulations in complementing limited NMR data for small peptides is demonstrated by an application to the important cell adhesion peptide Arg-Gly-Asp-Trp (RGDW) and its synthetic analogue, D-Arg-Gly-Asp-Trp (D-RGDW). The results of an earlier NMR study of these peptides were interpreted in terms of a type II′ β-turn conformation (Kieffer, B.; Mer, G.; Mann, A.; Lefèvre, J. F. *Int. J. Pept. Protein Res.* **1994,** *44,* 70−79). The present simulations provide additional insight into the solution structure of the RGDW and D-RGDW peptides by identifying extended conformations of both peptides in aqueous solution that are also compatible with the NMR data. The extended conformations have similar values for the NMR observables as the type II′ β-turn, including the pH titration behavior, coupling constants, ROESY proton distances and pK_a values of the Asp side chain and the C-terminal end. Thus it is difficult to distinguish the two conformations by NMR alone. Poisson−Boltzmann continuum electrostatics calculations for the conformations from the simulations show that the electrostatic free energies of solvation are about the same for the two peptide conformations. There is also good agreement between the NMR data and the pK_a values calculated using the continuum electrostatics model. The present study proposes that a mixture of extended and turnlike conformations gives the best agreement with the experimental results for both the RGDW and the D-RGDW peptides.

I. Introduction

In recent years there has been a significant interest in proteins and small, biologically active peptides containing the sequence Arg-Gly-Asp (RGD). This tripeptide sequence was identified as a fundamental unit involved in recognition by a number of cell surface proteins[1] of a variety of glycoproteins which play an important role in cell adhesion. Studies showed that small peptides containing the RGD sequence are recognized by the integrin cell surface receptors with high affinity and can compete effectively with the native protein for receptor binding.[2−4] The behavior of the peptides is sensitive to their sequence;[5,6] for example, substituting the glycine with alanine or the aspartic acid with glutamic acid eliminates adhesion activity.

Nuclear magnetic resonance (NMR) spectroscopy and X-ray crystallography have been used to elucidate the structures of the RGD tripeptide in cell adhesion proteins,[7−9] in a number of potent RGD containing integrin inhibitors isolated from the venom of various vipers[10−13] and leeches,[14] in virus coat proteins;[15,16] and in small peptides containing the RGD sequence,[6,17−23] as well as small synthetic molecules containing the RGD moiety.[24−26] The NMR studies indicate that the sequence has a propensity to form a reverse turn, although in several crystal structures it exists in extended conformations. In many of the NMR studies, the detailed structure has not been fully determined, in part because the loop involving RGD appears to be flexible.[9] Thus, the available data are not conclusive as to the conformational requirements for cell adhesion activity of RGD, though it is likely that a turn conformation is required and that extended forms have to be sufficiently flexible to form such a turn.

The linear peptides RGDW, D-RGDW, and cyclic dipeptide c(RGDW)$_2$, have been studied by multidimensional NMR spectroscopy.[23] The results suggest that the linear peptides form a type II′ β-turn with the Gly and Asp residues in positions 2 and 3 of the turn, respectively. This is in accord with the analysis of such turns in proteins.[27−30] Evidence for fast internal motions was found that suggested that the linear tetrapeptide has considerable flexibility in solution,[31] so there is the possibility that conformations other than the turn contribute to the average structure. Since NMR measurements often cannot by themselves distinguish multiple conformations when exchange among them is rapid on the NMR time scale,[32−34] these other conformations could not be identified. This makes it important to supplement NMR data by simulations.[35,36] The study presented here employs unconstrained molecular dynamics simulations to probe the structure and conformational dynamics of the linear peptides RGDW and D-RGDW. The simulation results are compared with the results from the NMR experiments, including the pH titration behavior, coupling constants, and ROESY proton distances. Continuum electrostatic models[37−39] are used to calculate the pK_a values of the Asp and the Trp residues in (D)RGDW using the structures from the simulations. These results are compared with the parameters determined from the NMR experiments.

* Corresponding authors. E-mail: rstote@chimie.u-strasbg.fr. E-mail: marci@brel.u-strasbg.fr.

† Laboratoire de Chimie Biophysique.

‡ Ecole Supérieure de Biotechnologie de Strasbourg.

§ This paper is dedicated to the memory of Jean-François Lefèvre. (1948-1999)

|| Department of Chemistry.

10.1021/jp992147m CCC: $19.00
Published on Web 01/29/2000

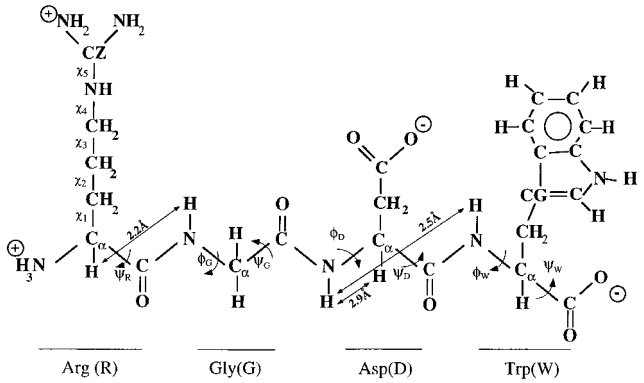

Figure 1. Definition of Dihedral Angles and ROE distances for RGDW.

The comparison between the simulation results and the experimental results shows that the NMR data do not define a unique structure for the RGDW peptide but that the NMR data is compatible with both turn and extended conformations in solution. It is proposed that a mixture of turn and extended conformations of the RGDW peptide, as suggested by the simulations, gives the best fit to the NMR data. Finally, a conformational analysis used in conjuction with the available structural data suggests factors that are important for the biological activity of the RGDW and D-RGDW peptides.

The simulation methodology is described in section II and the results and discussion are presented in section III. Section IV presents the conclusions. Tables of mean dihedral angles and their fluctuations from the simulations along with a table of mean dihedral angles from the cluster analysis are provided in the Supporting Information.

II. Methods

Molecular Dynamics Simulations. Version 22 of the CHARMM program,[40] with a preliminary version of the CHARMM22 all-atom potential function,[41] was used for all calculations. On the basis of the NMR results, the starting structures of the RGDW and D-RGDW peptides were built in an ideal type II′ β-turn conformation with the QUANTA [Molecular Simulations, Inc.] program. To construct the D-Arg, the internal coordinate definitions for two improper dihedral angles[40] centered on the Cα atom of Arg were modified; these impropers, N−C−*CA−CB and N−C−*CA−HA, define the orientation of the Hα and the Cβ atoms. All other internal coordinates and parameters remained unchanged. Hydrogen atom positions were determined by use of the HBUILD facility[42] in the CHARMM program. An energy minimization of 500 steps using the ABNR minimizer[40] was performed on the isolated peptide to remove short van der Waals contacts and strained valence angles. During the minimization, force constants of 2000 kcal/mol rad^2 were placed on the peptide backbone dihedral angles to constrain the peptide to a type II′ β-turn; no constraints were placed on the side chain atoms or angles. The nonbond pair list included all pair interactions (i.e., no cutoff was used) and electrostatic interactions were treated using an r-dependent dielectric constant[43,44] during the preliminary vacuum energy minimizations;[45] the energy minimized structures for RGDW and D-RGDW are shown in Figure 1. The root-mean square differences between the initial and the energy minimized coordinate sets were 0.22, 0.24 Å for the backbone atoms and 0.92, 0.78 Å for the side chain atoms of RGDW and D-RGDW, respectively. The minimized structure was solvated with an equilibrated cubic box of a modified TIP3P water molecules[46,47] with dimensions of 31.1 Å. Waters overlapping the peptide were deleted; a total of 37 and 38 water molecules were removed from the RGDW and D-RGDW systems, respectively. The final system contained a total of 2959 atoms for the RGDW system (70 peptide atoms and 963 water molecules) and 2956 atoms for the D-RGDW system (70 peptide atoms and 962 water molecules). A 10 Å group-based cutoff was used and the nonbonded interactions were truncated with a switching function[40] between 7.0 and 8.5 Å. A 1 ps simulation at 100 K with the peptide fixed at its minimized structure was done to remove any strong repulsive interactions between the water and the peptide. The electrostatic interactions were treated with a dielectric constant equal to one in the presence of explicit solvent. The constraints fixing the peptide were then removed and a 15 Å group-based cutoff with a switching function between 10.0 and 14.5 Å was introduced; this cutoff model was used in all subsequent molecular dynamics simulations. The IMAGE facility in the CHARMM program was used to compose the minimum image convention with periodic boundary conditions, and the SHAKE algorithm[48] was used to constrain bonds between hydrogens and heavy atoms. A 3 ps molecular dynamics simulation was done during which the system was heated from 100 to 300 K by periodically reassigning the velocities from a Gaussian distribution. An equilibration phase of 3 ps followed, during which the temperature was monitored and the velocities were scaled when the temperature was $\pm$5 K from the desired temperature of 298 K. During the production phase, no velocity scaling was used. A time step of 1 fs was used in the dynamics calculation for the RGDW peptide. For the simulations of D-RGDW, a slightly different protocol was used. The system was heated over 20 ps followed by a 60 ps equilibration. In order to access longer time scale during the simulations of D-RGDW, a 2 fs time step was used. Four simulations of the RGDW peptide were performed (for 296, 123.5, 66, and 211 ps) using different initial velocity distributions. Three simulations of the D-RGDW peptide were performed, for 280, 480, and 780 ps.

To analysis the conformational data from the molecular dynamics trajectory, the ART-2′ clustering algorithm, implemented in the CHARMM program,[49] was used. This algorithm is based on a self-organizing neural net[50,51] and it produces a single, optimized partition of the trajectory data. The clustering algorithm describes the conformation of the peptide by a vector of N parameters; in the present study, the ϕ and ψ backbone dihedral angles for all residues and the χ1, χ2 side chain dihedrals for the Arg, Asp, and Trp residues are used. The cutoff "radius" for each simulation was chosen after visual inspection of the dihedral angle time series such that the resultant clusters reflect the major transitions in the dihedral angle time series. The cutoff radius varied from 55° to 70° for the different simulations. The clustering was done using only the production phase of the simulations.

Continuum Dielectric Calculations. A continuum dielectric model was employed to calculate the pK_a values of the titratable groups in the peptide[52,53] and the relative electrostatic free energies of solvation for different peptide conformers.[54] In these models, a solvated protein or peptide is represented as a low dielectric medium embedded in a high dielectric medium, which represents the solvent, and the linearized Poisson−Boltzmann equations are solved by numerical methods.[55] The total electrostatic free energy of a polar molecule is given by the sum of the free energy required to charge the molecule in vacuum ΔG_{coul} plus the electrostatic contribution to the solvation free energy ΔG_{Sol}. The value of ΔG_{coul} is calculated using the

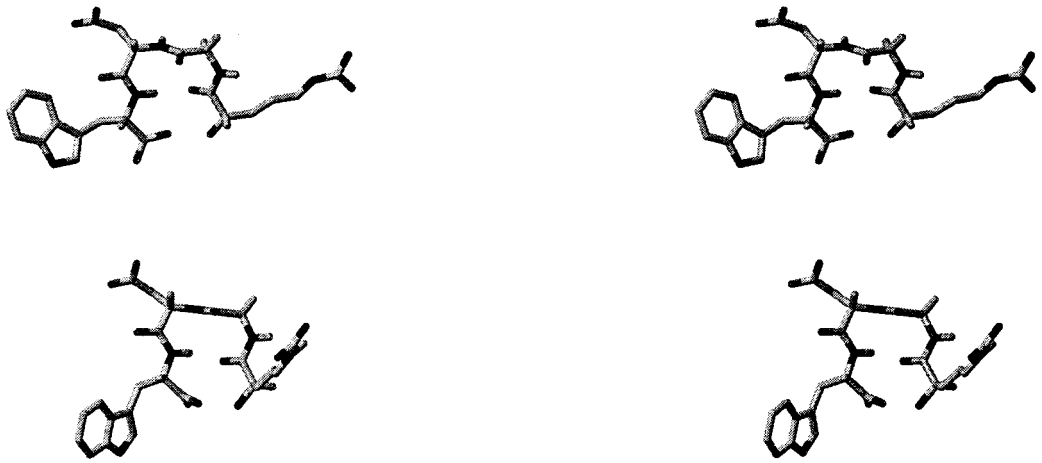

Figure 2. Stereoviews (cross-eyed) of RGDW (top) and D-RGDW (bottom) after energy minimization. Only backbone hydrogens are shown. The figure was made using the program MOLMOL.[77]

Coulomb term in the CHARMM potential energy function. The electrostatic free energy of solvating the conformer ΔG_{Sol} in a medium of dielectric 80, representative of an aqueous solution, was calculated using the continuum dielectric model. The relative free energy difference between the initial conformer in the series and each subsequent conformer i equals

$$\Delta\Delta G = [(\Delta G_{\mathrm{Coul}} + \Delta G_{\mathrm{sol}})_i - (\Delta G_{\mathrm{Coul}} + \Delta G_{\mathrm{Sol}})_{\mathrm{initital}}] \quad (1)$$

Details concerning this approach have been given in the literature.[38] In the present study, the UHBD program[56] with an interface to CHARMM and a module for evaluating pK_a values[57−59] were employed. The calculations were done assuming an internal dielectric constant of 20[59,60] and a grid spacing of 0.3 Å.

II. Results

(a) Molecular Dynamics Simulations. The simulations of RGDW and D-RGDW were started from an energy minimized type II′ β turn conformation based on the NMR data of Kieffer et al.[23] Backbone and side chain dihedral angle time series were used to characterize the conformational changes during the molecular dynamics simulations; see Figure 1 for the definition of dihedral angles in the RGDW peptide. The results from the RGDW simulation are presented first followed by the results from the D-RGDW simulations. A comparison of the simulation results with the experimental NMR results is then given. The final section presents the population/conformation analysis.

RGDW. After the energy minimization, the RGDW peptide remained in a type II′ β turn conformation with Gly(ϕ,ψ) of (60.3°, −119.7°) and Asp(ϕ,ψ) of (−79.9°,−0.0°); see Figure 2a. In the four simulations of RGDW, the peptide moved from an ideal II′ β turn to a distorted β turn conformation during the early stages of the simulation; for example, during the first 5 ps of the RGDW(1) simulation, Gly(ϕ,ψ) move from its initial values to (73°,−70°) and the Asp(ϕ,ψ) moved to (−75°,−79°); the dihedral angle time series for the Gly(ϕ,ψ) and Asp(ϕ,ψ) dihedral angles from the RGDW simulations are given in Figure 3. In the RGDW(1) simulation, a significant conformational transition occurs after 9 ps of production phase dynamics; the ϕ angle of Gly goes from about 60° to about −150° over a period of several picoseconds (Figure 3a). At about the same time the ψ angle of Gly goes from −75° to about −180°. There are no additional major backbone transitions until about 150 ps where the ψ angle of Gly starts to return to its original value of about −60°; at about the same time, the ψ angle of Asp (Figure 3a) goes from −60° to −180°. Significant motion of the side chains appears to be correlated with the backbone motion as expected from studies of protein conformational data;[61,62] see Figure 4. The χ1 of Arg and the χ1 of Asp undergo a conformational transition at roughly the same time as the transition in Gly ϕ angle. Similar distortions from an ideal conformation were observed in the early stages of the other three RGDW simulations. In RGDW(2) and RGDW(4) simulations, the peptide undergoes a transition from a turn conformation to an extended structure, in the simulation RGDW(2) (Figure 3b), this transition occurs at around 75 ps into the simulation and in the simulation RGDW(4) (Figure 3d), the transition occurs at around 100 ps into the simulation. In the simulation RGDW(3) (Figure 3c), the peptide moved from the β turn conformation early in the simulation, but it returned to a β turn conformation after several picoseconds.

The ART-2[1] clustering algorithm as implemented in the CHARMM program[49] was used to cluster the conformations by backbone dihedrals {Arg(ψ), Gly(ϕ,ψ), Asp(ϕ,ψ), Trp(ϕ)} and side chain (χ1, χ2) dihedral angles. A single family of clusters for RGDW was obtained from the four simulations. The individual conformations were presented in the order they appear in the dynamics trajectory and the dynamics trajectories were ordered as RGDW(2), RGDW(3), RGDW(4), and RGDW-(1). Four clusters were obtained using a cutoff radius of 70°; the mean dihedral angles of the different clusters, along with their populations, are given in Table 3 of Supporting Information. Clusters 1 and 2 represent conformers which are close to an ideal type II′ β turn; the extended conformations fall into clusters 3 and 4. Cluster 4 has the highest population, followed by cluster 2. Differences between the turn and extended conformers are mainly in the Gly ϕ and Asp ψ dihedral angles. Conformations of RGDW having the mean dihedral angles from the clusters were constructed and stereoviews are given in Figure 5A. Clusters 1 and 2 are clearly more turnlike than clusters 3 and 4.

Recently, molecular dynamics simulations with adaptive umbrella sampling of the potential energy were used to study the conformation of the RGDW peptide in explicit water.[63] Adaptive umbrella sampling is more efficient than conventional molecular dynamics for finding the accessible range of conformations under a given set of thermodynamic conditions.[64−66] It also provides the relative probabilites for the observed structures. In the simulations of the RGDW peptide, Bartels et al.[63] found that the most probable conformations in explicit solvent were

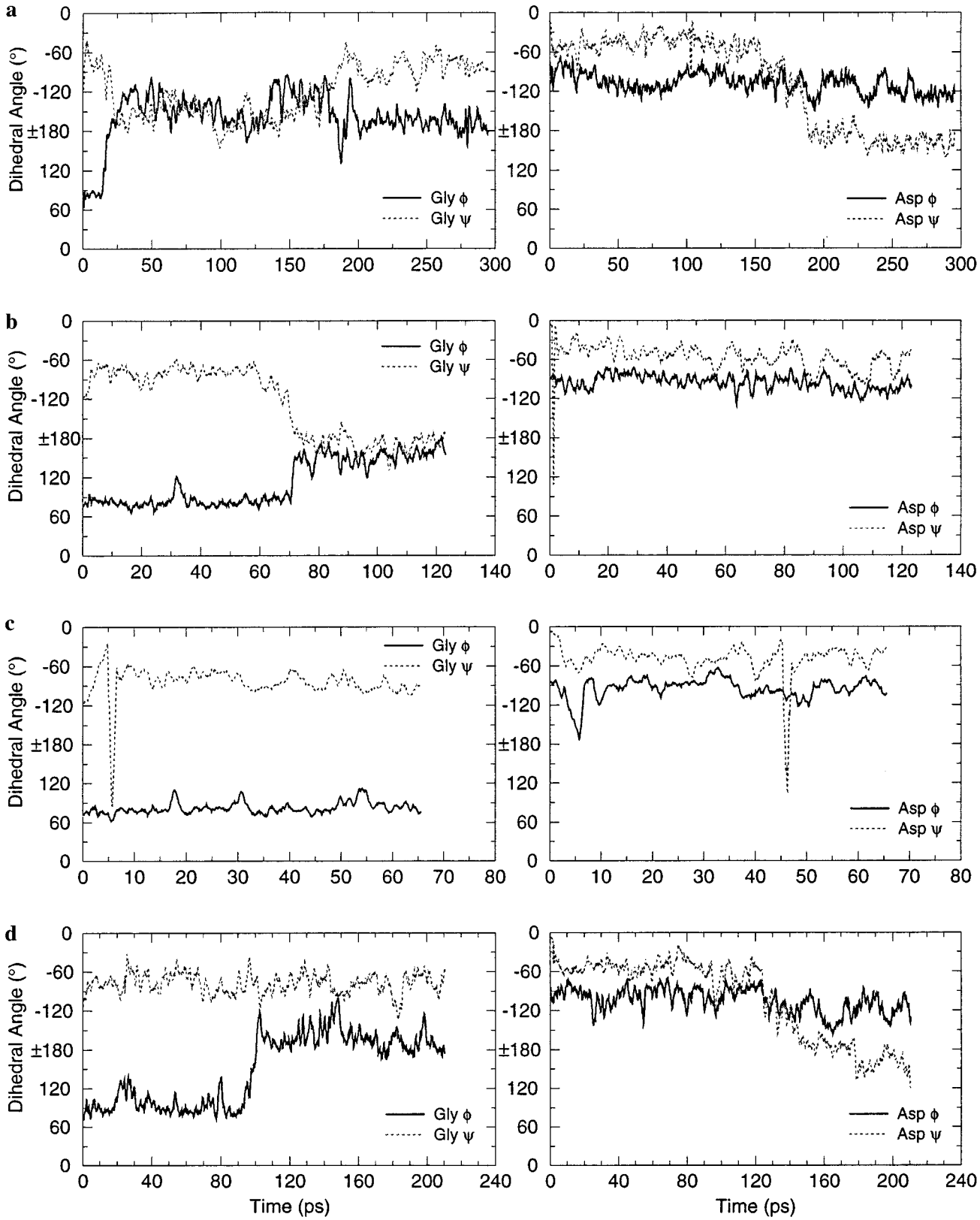

Figure 3. Gly and Asp dihedral angle time series from the RGDW simulations. From top to bottom, simulations RGDW(1) to RGDW(4).

extended although turnlike conformations also contributed to the ensemble.

D-RGDW. The three simulations of D-RGDW of 200, 400, and 700 ps of production phase dynamics are referred to as D-RGDW(1), D-RGDW(2), and D-RGDW(3), respectively. After energy minimization, the peptide was in an ideal type II′ β turn conformation (Gly ϕ and ψ of 60.1° and −120.0°, respectively and Asp ϕ and ψ of −80.1° and −0.1°, respectively), see Figure 2b.

In the D-RGDW(1) simulation (see Figure 6a for the dihedral angle time series), the peptide remains in a distorted turn conformation for the duration of the simulation; deviation from the ideal structure is due to the displacement of the ψ dihedral angle of Asp during the heating and equilibration phase of the

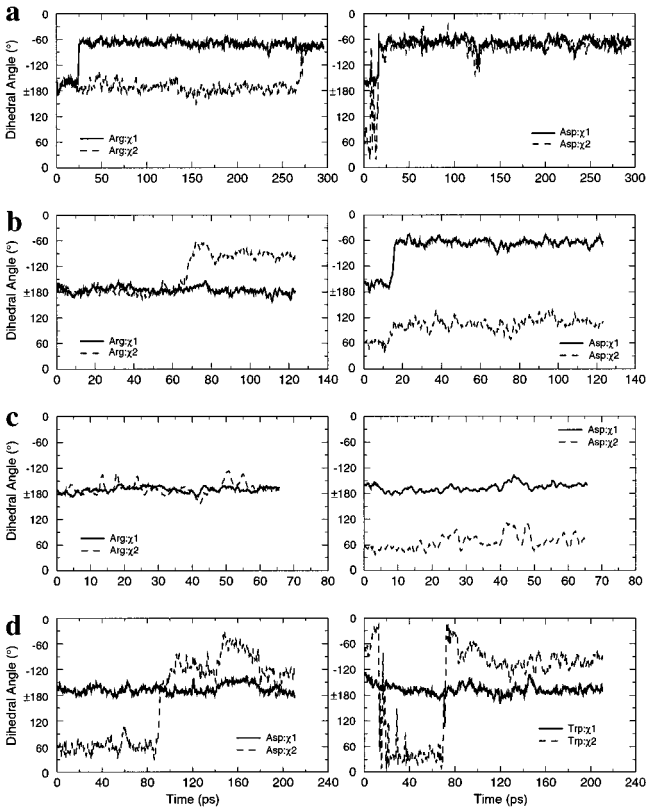

Figure 4. Side chain dihedral angles time series from the RGDW simulations. Only those side chain dihedral angles that undergo significant transitions are shown. From top to bottom, simulations RGDW(1) to RGDW(4).

TABLE 1: pK_a values for the Asp Side Chain and the C Terminal End Calculated Using the Continuum Dielectric Model

	Asp	Trp (C Terminal)
experiment	3.8	3.3
D-RGDW (β-turn)	4.07	2.70
RGDW (β-turn)	4.09	2.70
D-RGDW (1)[a]	4.02 (0.09)	3.78 (0.05)
D-RGDW (2)[a]	3.96 (0.01)	3.59 (0.01)
D-RGDW (3)[a]	3.94 (0.01)	3.79 (0.01)
RGDW[b]	3.91 (0.07)	3.52 (0.10)

[a] All structures from the simulations were used to calculate the average value and standard deviation. [b] Every 10th structure was used to calculate the averages from RGDW.

simulation. The other three dihedral angles which define the turn, the ϕ,ψ of Gly and the ϕ of Asp, remain close to their ideal values. Following the changes in the backbone dihedral angles, significant transitions in the $\chi 2$ side chain dihedral angles of Asp and Trp occur (Figure 7a). These side chain dihedral angles return to about their initial values over the course of the subsequent 100 ps.

In the simulations of D-RGDW(2) and D-RGDW(3), Figures 6b,c and 7b,c, the peptide opens to a more extended conformation during the equilibration and heating phase. In the D-RGDW-(2) simulation (Figure 6b), the ψ of Asp moves from its initial value at the beginning of the heating phase, $\sim 0°$, to $\sim -80°$; at around 100 and 350 ps, significant transitions in the $\chi 2$ of Asp occur (Figure 7b). At around 20 ps into the heating phase, there are major transitions in the Gly backbone dihedrals ϕ,ψ which go from $\sim 60°$ and $\sim -120°$, respectively, to about ± 180. Major transitions in the side chain dihedral angles of Asp and Trp occur throughout the simulation. In the D-RGDW(3) simulation (Figure 6c), the ϕ of Gly goes from $\sim 60°$ to $-150°$ and Gly ψ undergoes multiple transitions, but returns to about its initial value of $-120°$ during the production phase of the simulation during which multiple side chain dihedral angle transitions occur. The side chain dihedrals undergo multiple transitions (Figure 7c).

TABLE 2: Backbone Coupling Constants Calculated from the Simulations[a]

RGDW cluster no.	Gly $^3J_{HN-H\alpha_1}$	Gly $^3J_{HN-H\alpha_2}$	Asp ($^3J_{HN-H\alpha}$)	Trp ($^3J_{HN-H\alpha}$)
1	4.1	7.2	8.1	8.6
2	5.4	7.4	7.9	8.4
3	6.1	3.4	8.6	8.7
4	6.9	3.2	8.8	8.0
overall average	6.0	5.0	8.4	8.3
experiment	5.1	6.1	7.5	7.6
D-RGDW cluster no.	**Gly $^3J_{HN-H\alpha_1}$**	**Gly $^3J_{HN-H\alpha_2}$**	**Asp ($^3J_{HN-H\alpha}$)**	**Trp ($^3J_{HN-H\alpha}$)**
1	5.2	7.7	7.2	8.1
2	3.4	8.4	7.4	8.5
3	8.0	4.7	7.7	8.0
4	3.2	7.1	7.5	7.0
5	6.0	3.7	7.6	8.1
6	4.1	5.8	8.2	8.1
7	7.6	3.3	7.7	8.2
8	8.1	2.8	7.9	8.7
overall average	6.3	5.0	7.6	8.2
experiment	5.7	6.4	7.9	7.9

[a] Average values for each cluster, the overall average values, and the experimental values are given.

A single family of clusters for D-RGDW was obtained from the three D-RGDW simulations using the ART-2′ algorithm. The individual conformations were presented in the order they appear in the dynamics trajectory and the dynamics trajectories were presented in the order D-RGDW(1), D-RGDW(2), and D-RGDW(3). As in the previous analysis, the clustering was done using the backbone and side chain dihedral angles. Eight clusters were found using a cutoff radius of 60°. Of the eight clusters, cluster 1 is the most turnlike with backbone dihedral angles close in value to those of a type II′ β turn ((ϕ) Gly = 93.5, (ψ) Gly = −149.0; (ϕ) Asp = −85.3, (ψ) Asp = 174.0); the other clusters contain more extended structures. Although the ART-2′ algorithm is susceptible to convergence to a local minimum, previous studies have shown that when using dihedral angle criteria, similar sets of clusters resulted from random ordering of conformations.[49] Using the same cutoff criteria as above but with a different ordering of the trajectories, the cluster analysis was redone to check the dependence of the clusters obtained on the order in which the trajectories were presented to the algorithm. In all cases, either similar sets of clusters, or essentially the same clusters and populations, were found.

Conformations of the D-RGDW peptide were constructed using the mean cluster dihedral angles; stereoviews are presented in Figure 8. Relative to the RGDW peptide clusters (Figure 5), the D-RGDW clusters are less turnlike and have a higher proportion of clusters with extended conformations.

(b) Continuum Dielectric Calculations. The relative stability of the different conformers was determined from eq 1 and the continuum dielectric model.[54] The gas phase electrostatic energy ΔG_{Coul} was calculated using the CHARMM22 all atom force field with a dielectric constant ϵ equal to 20; the electrostatic part of the solvation free energy (ΔG_{Sol}) was calculated using the UHBD program. Every coordinate set was extracted from the production phase of the D-RGDW simulations, and the total electrostatic free energies (internal terms plus external terms)

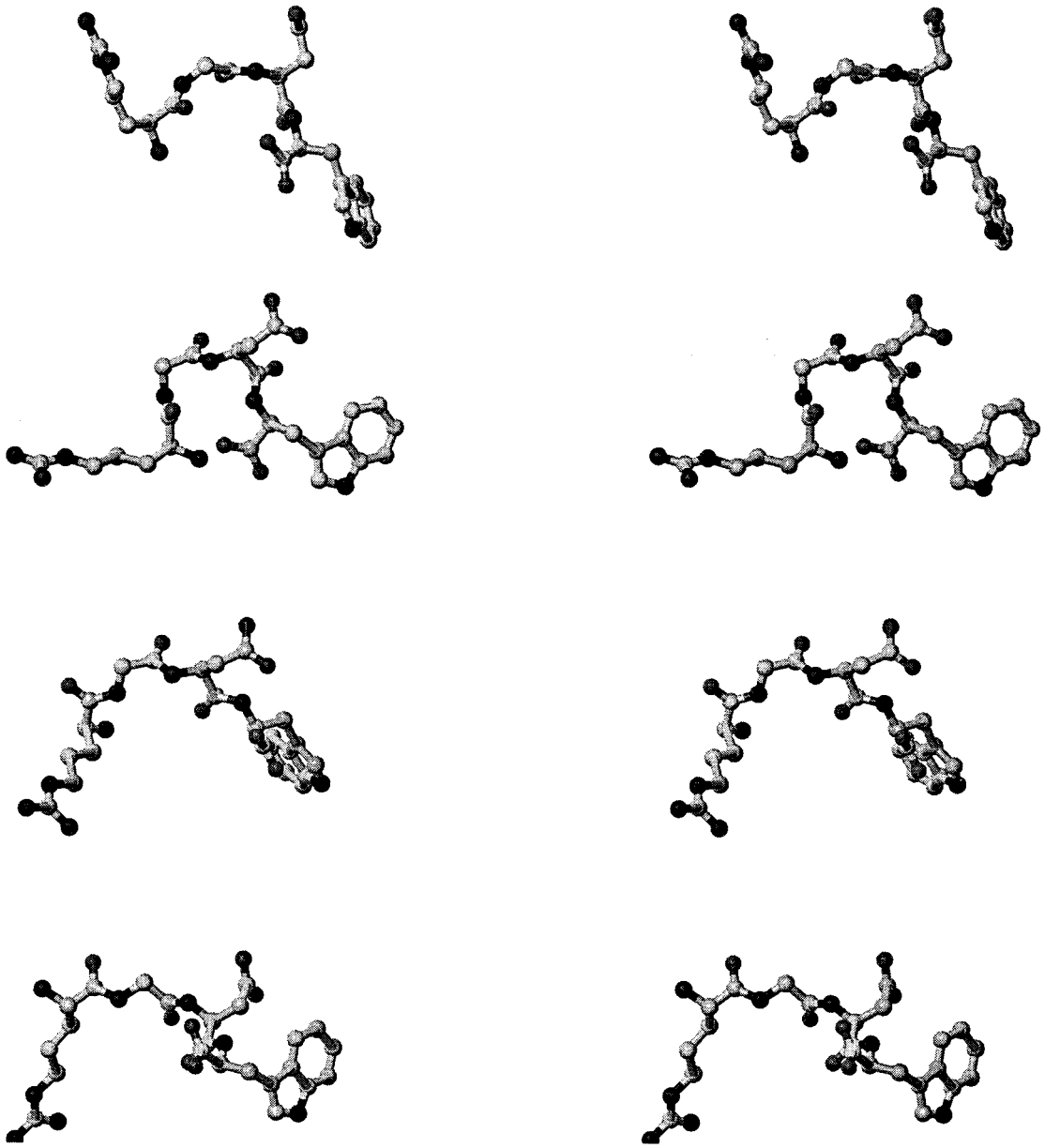

Figure 5. RGDW conformations constructed using the cluster dihedral angles in Table 3 of Supporting Information. (cross-eyed stereoview)

was calculated. The time dependence of the Coulomb energy ΔG_{Coul} and the solvation component ΔG_{Sol} (Figure 9) indicates that when there is a loss of stabilizing Coulomb interactions between groups in the peptide, there is a corresponding compensation by improved solvation. Thus, the total electrostatic solvation free energy time series (Figure 9) from each of the three simulations does not vary significantly, indicating that the different conformers are about equally stable in solution. Similar behavior was seen in the simulation of the peptide APDG.[67] These results, combined with the simulation results described in the previous section indicate that for the D-RGDW peptide, the turn and extended structures can both exist in solution. Similar calculations done for the RGDW peptide yield the same conclusions.

(c) Comparison with NMR Results. The structural features of two linear peptides which inhibit platelet aggregation: D-Arg-Gly-Asp-Trp and L-Arg-Gly-Asp-Trp have been investigated by ^{1}H and ^{13}C NMR.[23] An analysis of pH titration effects on chemical shifts, amide proton exchange, *J*-coupling constants and interproton distances from ROESY experiments were interpreted as showing the peptides adopt a type II′ β-turn in solution. Relaxation studies indicate the presence of fast internal motions which cannot be resolved by NMR.[31] In this section, we compare the simulation results to the experimental NMR results.

The pH titration studies of D-RGDW indicate that titration of the C-terminal group with a pK_a of 3.3 affects the ^{13}C chemical shift of the Arg carbonyl carbon and the chemical shifts of the Arg protons. These changes were attributed to changes in the electrostatic field around the carbon due to changes in the protonation state of the C terminal end. In addition, for the ^{13}C chemical shift of the Arg carbonyl carbon, a change to a hydrogen bond between the amide hydrogen of the Trp and the carbonyl oxygen of Arg was suggested as a second possible factor. For the Arg side chain protons, an increase in magnitude of the chemical shifts was observed when going from the β to γ protons. This was attributed to a possible interaction between the positively charged guanidinium group of Arg and the C-terminal end of the peptide.[31] In the simulations of the RGDW and D-RGDW peptides, the O:Arg-HN:Trp hydrogen bond occurred rarely during the production phase of the simulations; this hydrogen bond was present only 3.2% of the time in the

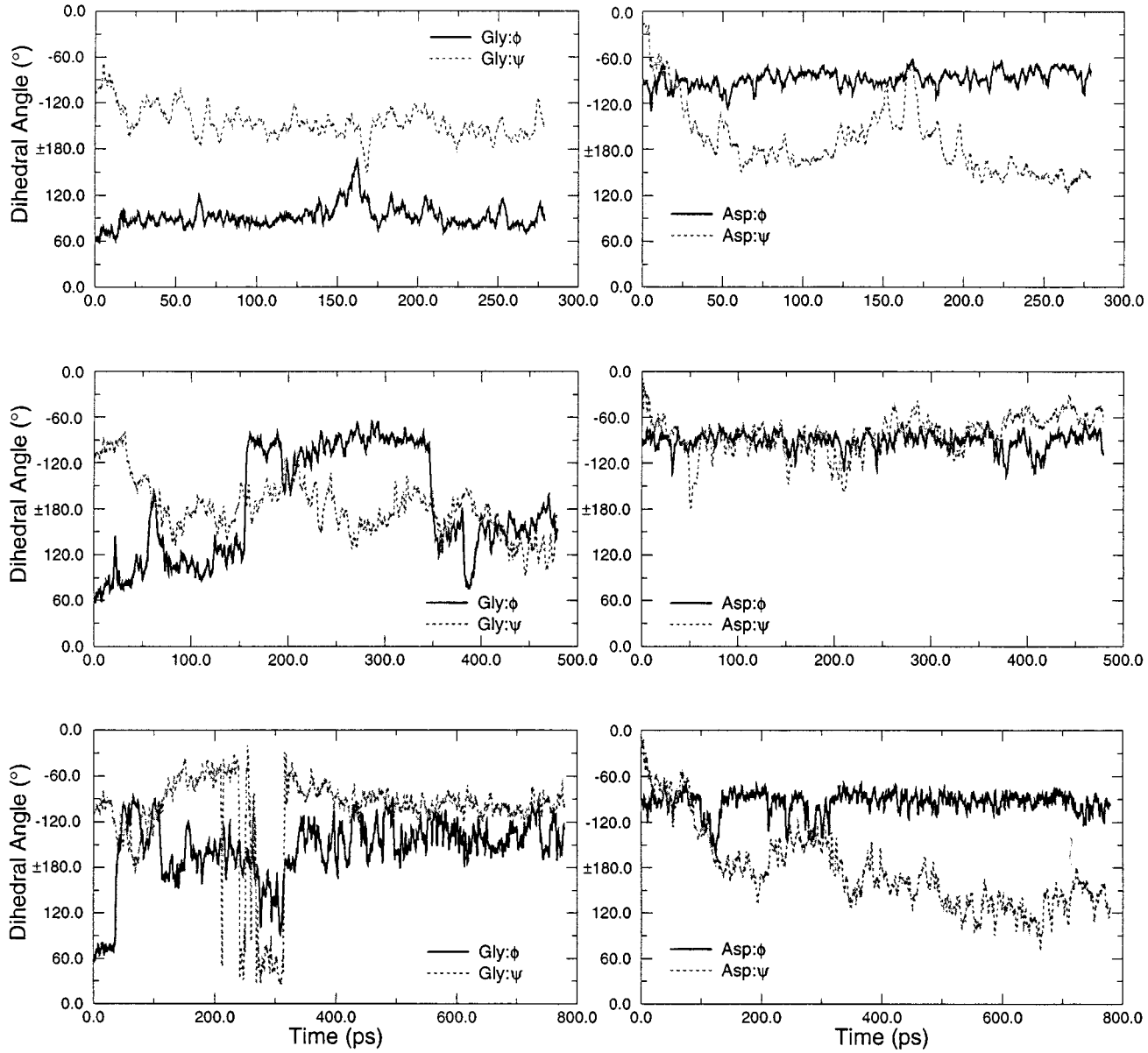

Figure 6. Gly and Asp dihedral angle time series from the D-RGDW simulations. From top to bottom, simulations D-RGDW(1) to D-RGDW(3).

RGDW trajectories and 0% of the time in the D-RGDW trajectories. The hydrogen bonds were calculated using the criteria of 4.5 Å and 90° for the heavy atom interatomic distance and the angle of deformation from linearity, respectively. Chemical shifts are sensitive to the electrostatic environment,[68] so the ^{13}C chemical shift of the Arg carbonyl carbon is sensitive to the C-terminal end position. In the molecular dynamics simulations of both peptides, the carboxy terminal oxygen was mostly more than 6 Å from the Arg:NH of the guanidinium group; only infrequently did the distance drop below 6 Å during the production phase. From the simulations, then, it seems unlikely that the changes in Arg side chain proton chemical shifts can be attributed solely to the interaction between the carboxy terminal oxygen and the guanidinium group. The simulations suggest another interaction that was not considered in the NMR experiments. In all three D-RGDW simulations, the distance between the Arg and Trp side chains, as monitored by the distance between the Arg:C_ζ side chain carbon and the Trp:C_γ side chain carbon, decreased relative to the distance between the two side chains after energy minimization. This suggests that the ring current field of the Trp ring could affect the chemical shifts of the Arg protons: in the D-RGDW(1) simulation, the distance dropped to below 7 Å; in the D-RGDW-(2) simulation, the distance was sometimes under 10 Å; and in the latter part of the D-RGDW(3) simulation, the distance was below 6 Å. The distances between the Arg protons and the Trp ring carbons ranged from 2.4 to ~5.0 Å. These results indicate that while the observed chemical shift effects may be due directly to changes in the protonation state of the C terminal end, ring current effects in the extended peptide conformations should also be considered.

The pK_a values of 3.8 and 3.3 were determined for the Asp side-chain carboxylic group and the C-terminal carboxylic group of D-RGDW, respectively. Continuum dielectric models were used to calculate the pK_a values of the Asp and Trp carboxylic groups; every conformation from the production phase of the three D-RGDW simulations and every 10th structure from the RGDW(1) simulation were used in the continumm model calculations of the pK_a; the average values and rms fluctuations are given in Table 1. The average values for the pK_a of Asp from the simulations of RGDW and D-RGDW are slightly higher than the experimental values (3.9−4.1 vs 3.8, respectively). The average values for the C terminal end are all higher than the experimental value of 3.3; the average values range from 3.5

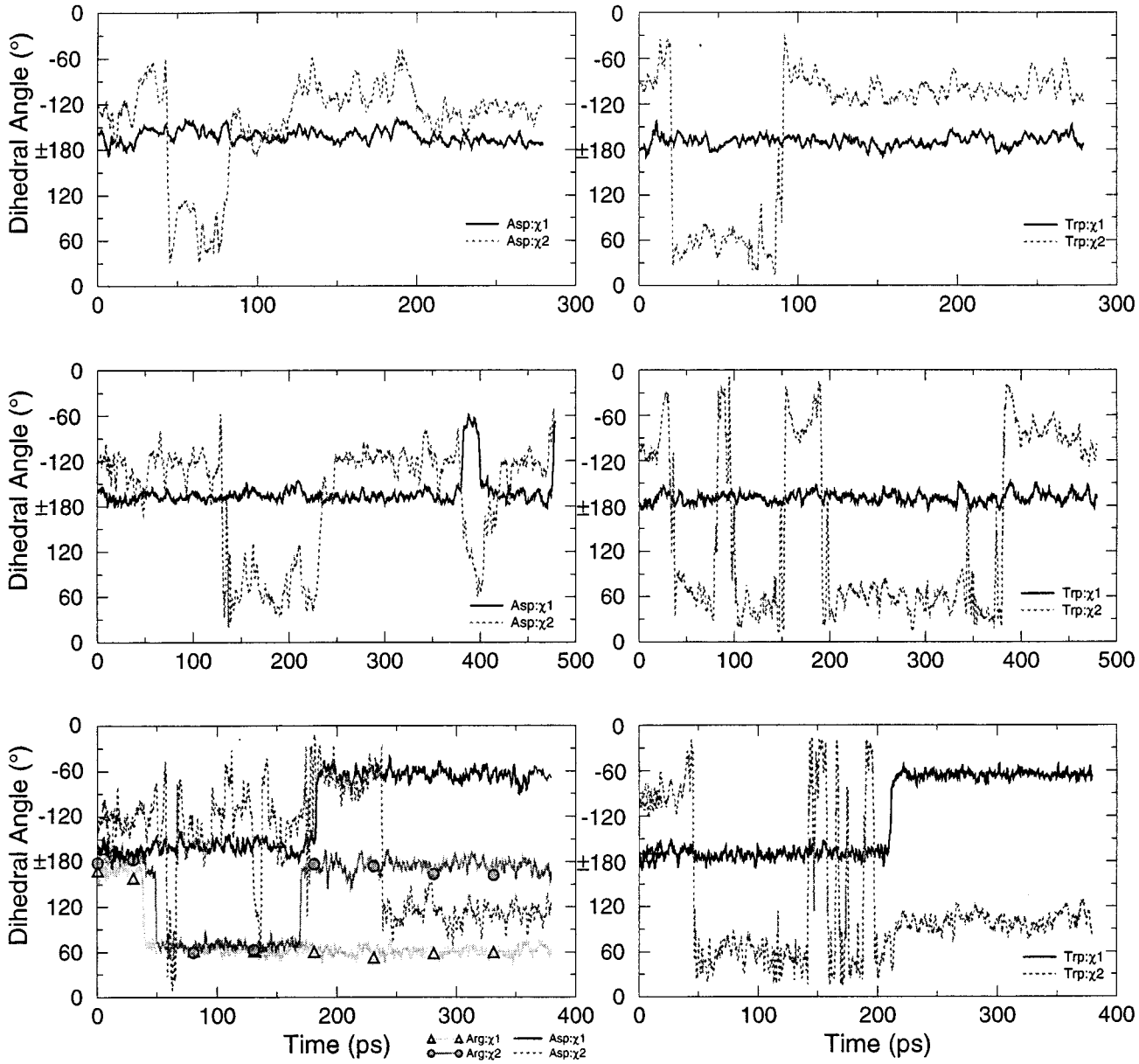

Figure 7. Side chain dihedral angles time series from the D-RGDW simulations. Only those side chain dihedral angles that undergo significant transitions are shown. From top to bottom, simulations D-RGDW(1) to D-RGDW(3).

to 3.8. However, these values are in better agreement with experiment than the C terminal end pK_a value calculated with the RGDW and D-RGDW peptides in an ideal type II′ β turn, where the C-terminal carboxylic group is in a salt bridge with the N-terminal NH_3^+ group (pK_a = 2.7).

The spin−spin coupling constants $^3J_{HnH\alpha}$ and $^3J_{H\alpha H\beta}$ provide information concerning the structure through the general relations

$$^3J_{HNH\alpha} = 6.4\cos^2\theta - 1.4\cos\theta + 1.9 \quad (2a)$$

$$^3J_{H\alpha H\beta} = 9.5\cos^2\theta - 1.4\cos\theta + 1.9 \quad (2b)$$

between ^3J and the angle θ;[69] $\theta = |\phi - 60|$ for $^3J_{HNH\alpha}$ and $^3J_{HNH\alpha 2}$, $\theta = |\phi + 60|$ for $^3J_{HNH\alpha 1}$, $\theta = |\chi - 120|$ for $^3J_{H\alpha H\beta 1}$, and $\theta = |\chi|$ for $^3J_{H\alpha H\beta 2}$. The coefficients in eq 2 were taken from ref 70 and from ref 71 for 2a and 2b, respectively. Coupling constants for the torsion angle ϕ and $\phi_{H\alpha H\beta}$ were measured in the NMR experiments for the Gly, Asp, and Trp residues. The corresponding dihedral angles were calculated for each conformation in the molecular dynamics simulations of RGDW and D-RGDW; the $^3J_{HNH\alpha}$, $^3J_{H\alpha H\beta}$, and $^3J_{H\alpha H\beta 2}$ coupling constants were then calculated via eqs 2 and averaged over the different clusters; the average values from the RGDW and D-RGDW simulations are given in Tables 2 and 3. Table 2 gives the calculated coupling constants for the backbone dihedral angles; an overall average value was obtained by making a weighted average over the trajectory, where the weighting factor reflected the relative populations. In both the RGDW and D-RGDW simulations, the average values are similar to the experimental values, although no single cluster gives good agreement with all of the experimental values. The largest discrepancy is for the Gly $^3J_{HNH\alpha}$ coupling constant. Table 3 gives the calculated J coupling constants for the side chain dihedrals. For the RGDW peptide, the agreement between the calculated values and the experimental values is reasonably good.

Short-range ROESY and NOESY cross peaks often provide the most unambiguous information concerning the secondary structure of a peptide or protein, although this is not true for

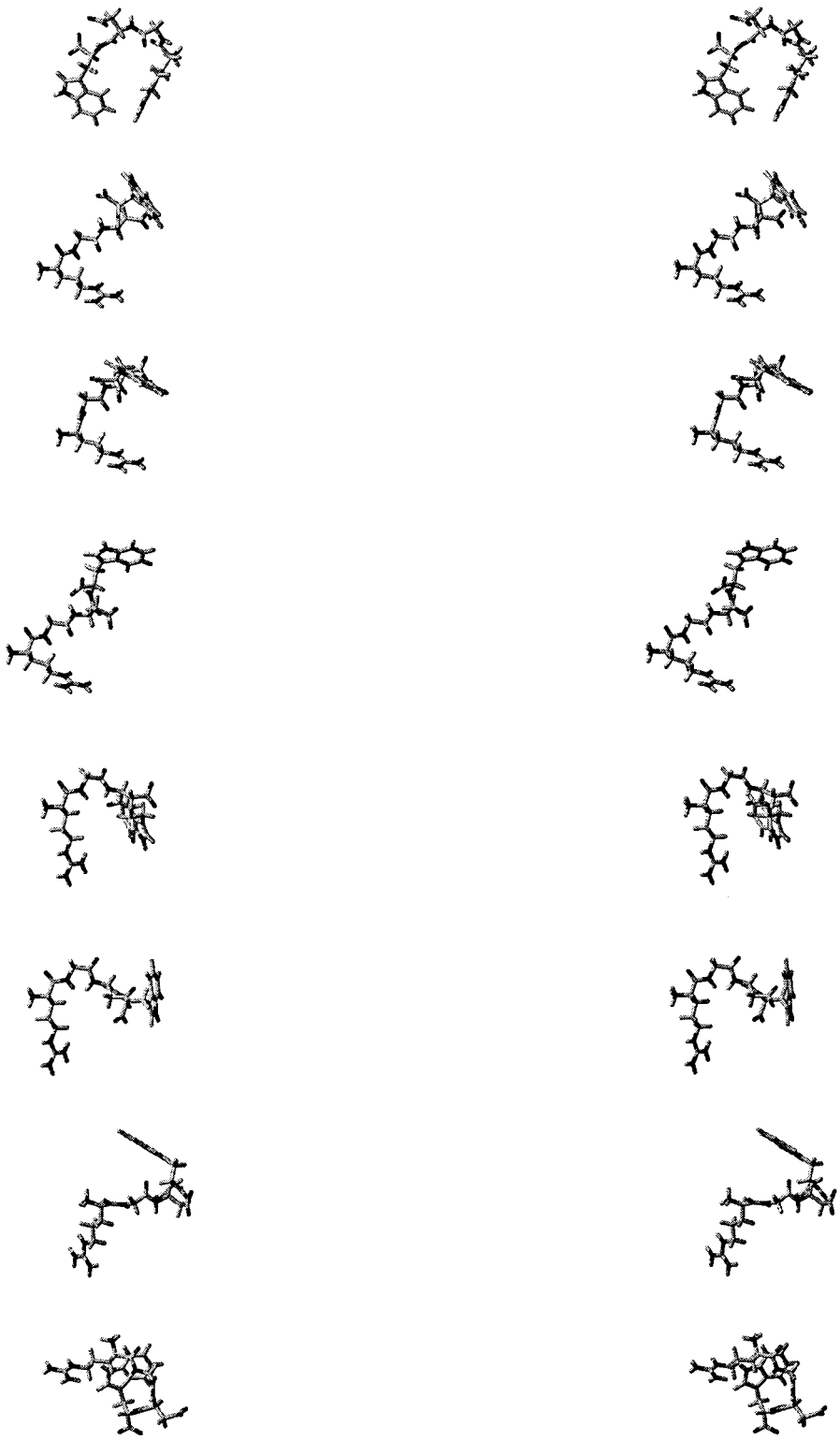

Figure 8. D-RGDW conformations constructed using the cluster dihedral angles in Table 3 of Supporting Information. (cross-eyed stereoview).

the RDGW peptide. The experimental observation of ROE connectivity between the proton pairs Hα(Arg)-HN(Gly), HN-(Asp)-Hα(Asp), and HN(Asp)-HN(Trp) is in accord with a significant population of a type II′ β-turn; for convenience, the distances obtained from the ROE measurements are shown in Table 4 and Table 5 for the RGDW peptide and for the D-RGDW peptide, respectively. The corresponding distances calculated from the simulations are similar in many of the different clusters. The simulation averaged distances are also listed in Tables 4 and 5. There is good agreement between the experimental and calculated distance between Asp:Hα-Asp:HN. The distance between Arg:Hα-Gly:HN from the simulations is shorter than that between Asp:Hα-Asp:HN which is consistent with the experiments, but no cluster average has a distance as short as the experimental value. For the distance between Asp:HN-Trp:HN, the overall average values are longer than the experimental values, but some individual clusters in the RGDW simulation have average values close to experiment. A strong ROE peak was experimentally observed between the amide proton of Asp and both geminal protons of Gly, indicating that

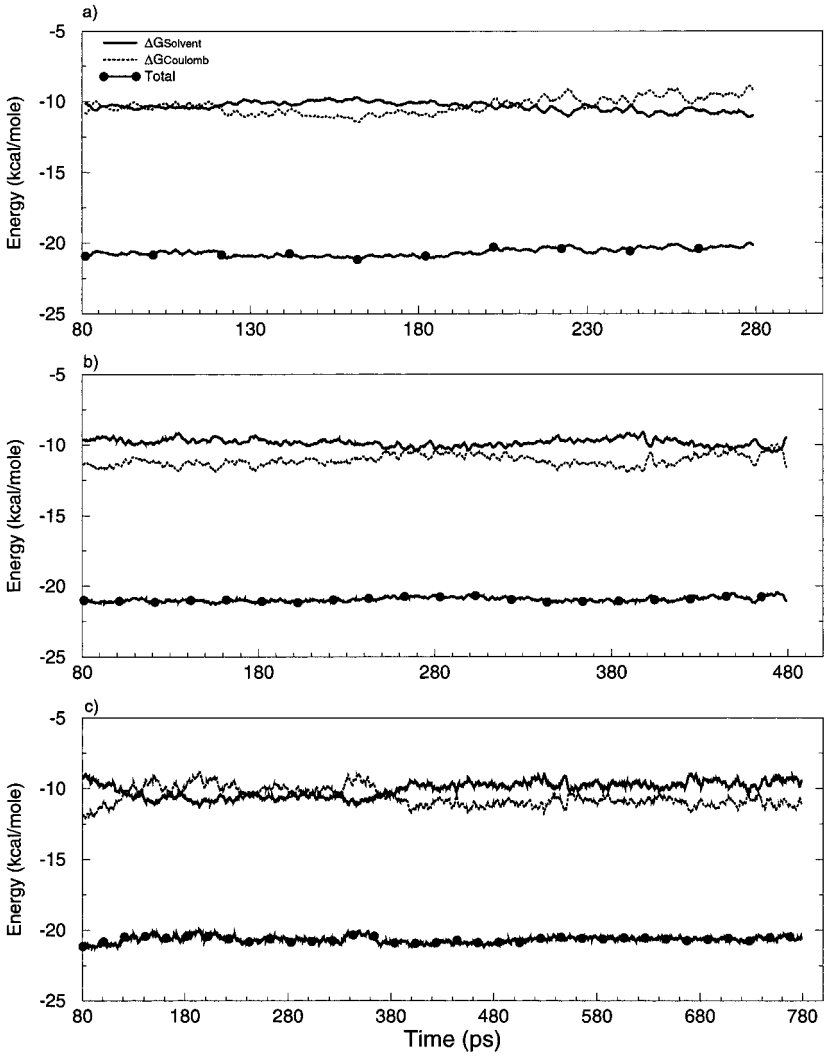

Figure 9. Time series for the solvation free energies calculated from the Poisson−Boltzmann equation. For the three simulations (a) D-RGDW(1), (b) D-RGDW(2), (c) D-RGDW(3).

these protons point in the same general direction. A precise distance could not be obtained because of spin diffusion even at low mixing times and distortion of the peak shapes due to strong scalar coupling (HOHAHA transfer) (Kieffer, B. Personal communication.). The simulations show that the distances are sufficiently short that one would expect strong ROEs from most of the clusters and that there is little variation between clusters. One cross peak that is generally used to indicate a β-turn conformation is between the α proton of residue 2 and the amide proton of residue 4.[33] Depending on the type of turn, this distance may vary from 3.3 to 3.6 Å and so would be expected to be of medium strength. In the experiments, this cross peak between the α protons of Gly and the amide proton of Trp was not observed and in the simulations the corresponding cluster averaged distances varied between 4.6 and 6.9 Å for the $H\alpha_1$ and $H\alpha_2$, respectively (Tables 4 and 5).

The experiments on the D-RGDW peptide indicated that the Trp amide proton is in slow exchange with the solvent. Changes in its rate of exchange as a function of pH are about 100 times smaller than would be expected for a fully accessible amide proton, even when taking into consideration the proximity of the Trp amide proton to the C terminal end of the peptide. This led to the conclusion that the Trp amide proton is protected from exchange by hydrogen bonding, presumably with the arginine carbonyl group.[23] However, as presented above, this hydogen bond was present in only 3.2% and in 0% of the trajectory time frames of the RGDW and D-RGDW simulations, respectively. However, the simulations of D-RGDW suggest

TABLE 3: Side Chain Coupling Constants Calculated from the Simulations[a]

	ARG		ASP		TRP	
RGDW cluster no.	$^3J_{\alpha\beta_1}$	$^3J_{\alpha\beta_2}$	$^3J_{\alpha\beta_1}$	$^3J_{\alpha\beta_2}$	$^3J_{\alpha\beta_1}$	$^3J_{\alpha\beta_2}$
1	3.3	12.4	12.4	3.3	2.7	12.0
2	2.7	12.2	3.0	11.4	3.1	11.3
3	2.6	12.0	2.6	11.6	2.8	12.0
4	11.9	3.1	12.1	3.0	12.3	3.6
average	6.6	8.4	8.1	6.8	6.8	8.3
experiment	6.5	6.5	4.9	8.7	5.2	6.9
	ARG		ASP		TRP	
D-RGDW cluster no.	$^3J_{\alpha\beta_1}$	$^3J_{\alpha\beta_2}$	$^3J_{\alpha\beta_1}$	$^3J_{\alpha\beta_2}$	$^3J_{\alpha\beta_1}$	$^3J_{\alpha\beta_2}$
1	4.8	12.3	2.4	11.6	2.7	12.1
2	4.2	12.3	2.5	12.2	2.9	12.3
3	4.8	11.8	2.4	11.9	2.6	12.1
4	4.8	11.4	4.1	10.1	2.6	12.0
5	4.1	3.3	2.2	11.4	2.8	12.4
6	3.9	3.5	2.1	10.9	2.9	12.4
7	4.0	3.6	10.5	4.6	6.5	8.5
8	3.9	3.6	12.4	3.2	12.5	3.1
average	4.3	7.6	5.6	8.9	5.3	9.8
experiment	6.2	7.6	5.3	8.5	5.5	7.4

[a] The average values for each cluster, the overall average values, and the experimental values are given.

TABLE 4: Average Interproton Distances (angstroms) Calculated from the RGDW Simulations[a]

cluster no.	population	R:Hα-G:HN	D:HN-D:Hα	D:HN-W:HN	D:HN-G:Hαl	D:HN-G:Hα2	W:HN-G:Hαl	W:HN-G:Hα2
1	1003	2.36	2.92	2.70	2.60	3.17	4.74	5.32
2	1779	2.36	2.91	2.55	2.44	3.51	4.63	5.44
3	1146	3.62	2.92	4.11	2.45	3.54	6.17	6.72
4	2797	2.52	2.94	3.85	2.41	3.27	5.69	6.22
average		2.87/2.59	2.93/2.92	3.64/3.04	2.46/2.40	3.38/3.29	5.50/5.01	6.07/5.76
experiment		2.2	2.9	2.5				

[a] Average values for each cluster are given; the distances were calculated as $\langle r^6\rangle^{1/6}$. The two average values given are the average over each conformation in the trajectory and the weighted average over each cluster, respectively.

TABLE 5: Average Interproton Distances (angstroms) Calculated from the D-RGDW Simulations[a]

cluster no.	population	R:Hα-G:HN	D:HN-D:Hα	D:HN-W:HN	D:HN-G:Hαl	D:HN-G:Hα2	W:HN-G:Hαl	W:HN-G:Hα2
1	949	2.38	2.88	4.47	2.34	3.04	6.22	6.64
2	506	2.36	2.89	3.30	2.78	2.61	5.26	5.63
3	1098	3.62	2.89	3.43	2.62	2.87	5.36	6.00
4	594	2.46	2.89	2.89	3.02	2.55	4.82	5.05
5	959	2.55	2.88	4.38	2.92	3.51	6.62	6.76
6	299	2.58	2.90	4.28	3.33	3.23	6.87	6.57
7	673	2.62	2.90	4.54	2.36	3.51	6.43	6.74
8	1422	2.55	2.92	4.46	2.29	3.46	6.04	6.19
average		2.89/2.64	2.90/2.89	4.21/3.95	2.70/2.53	3.24/3.10	6.10/5.86	6.33/6.12
experiment		2.2	2.9	2.5				

[a] Average values for each cluster are given; the distances were calculated as $\langle r^6\rangle^{1/6}$. The two average values given are the average over each conformation in the trajectory and the weighted average over each cluster, respectively.

another mechanism of hydrogen protection; in these simulations, the amide proton of tryptophan interacts with the Asp side chain oxygens. Analysis of the trajectories indicate that there is a significant population of conformations where the Trp:HN-Asp:O_δ distance is 2 Å or less in the D-RGDW simulations; a less significant population was found in the RGDW simulations.

(d) Population and Database Analysis. If an equilibrium between the different conformations (clusters) is assumed, the value of an experimental observable, A^{exp} (the interproton distance or the scalar coupling constant, for example), can be expressed as a linear combination of the values for each conformation weighted by their relative populations

$$A^{exp} = \sum_\sigma P_\sigma A^{cal} \tag{3}$$

where A^{exp} is the value of the experimental observable and A^{cal} is the calculated value of the observable for conformation σ; P_σ is the relative population of conformation σ. Subject to the constraints that the sum of the relative populations must equal 1, e.g., $\Sigma P_\sigma = 1$, and that the individual populations must lie between 0 and 1, it is possible to estimate the relative populations by treating the problem as a constrained least squares minimization. Although all the conformations from the simulations could, in principle, be used, the magnitude of the problem is reduced by using the cluster averaged values calculated in the previous section. Alternative methods of population analysis have been suggested.[72−75] Included in this analysis are the $^3J_{HNH\alpha}$ and $^3J_{H\alpha H\beta}$ coupling constants (Tables 2 and 3) and the interproton distances (Tables 4 and 5 for RGDW and D-RGDW, respectively). The constrained least squares equations were solved using a bounded variables least squares algorithm.[76] The relative populations of the RGDW and D-RGDW clusters are given in Tables 4 and 5, respectively. The best fit to all of the experimental data was obtained with a mixture of turn and extended conformations for both RGDW and D-RGDW; for RGDW, relative populations of 0.62 and 0.38 for clusters 2 and 4 were found, and for D-RGDW, the populations 0.14, 0.08, 0.03, 0.30, 0.00, 0.13, 0.00, and 0.33 were found for clusters 1−8, respectively.

Experimental studies suggest that the cell adhesion activity of the RGD moiety is critically dependent on its conformation. In a study by Müller et al.,[6] for example, the structure of 18 cyclic RGDF peptides were determined by 2D NMR spectroscopy and restrained molecular dynamics simulations; their activities were characterized by IC_{50} values and were compared to the linear peptide GRGDS and to fibrinogen, vitronectin and fibronectin. The differences in activity of the cyclic peptides ranged over 5 orders of magnitude. From an analysis of interproton distances and the pseudo-dihedral angle defined by ϕ[Cβ(R)−Cα(R)−Cα(D)−Cβ(D)], it was shown that slight changes in conformation can lead to significant differences in activity as measured by IC_{50} values. Of the eighteen compounds tested, the majority compounds had a ϕ[Cβ(R)−Cα(R)−Cα(D)−Cβ(D)] angle between ±60°, the most active ones had angles around 30°. Pseudodihedral angle values close to zero indicate an parallel alignment, i.e., the side chains are pointing in the same direction.

From the present simulations, the relative orientation of the Arg and Asp side chains was measured by the pseudo-dihedral angle, ϕ[Cβ(R)−Cα(R)−Cα(D)−Cβ(D)]. The values of ϕ[Cβ(R)−Cα(R)−Cα(D)−Cβ(D)] in the RGDW simulations ranged from −60° to 180° with a dominant peak around 0°. Of the four RGDW simulations, one showed no population in the "active" region around 0.0° and a large distribution between 60° and 180°; the other three RGDW simulations sample conformations in the "active" region. In the D-RGDW simulations, there was a significant distribution of ϕ[Cβ(R)−Cα(R)−Cα(D)−Cβ(D)] centered at about −30° which drops to zero at the boundaries of the "active" region. These results indicate that the RGDW and D-RGDW peptides share some conformational features with the active cyclic peptides studied by Müller et al.[6] This may provide additional insight into the activity of RGD containing peptides. The details of this analysis will be presented elsewhere (Stote, R. et al., in preparation.).

III. Conclusions

The RGD sequence is implicated as being critically important in adhesion processes. This paper is concerned with the two

linear peptides Arg-Gly-Asp-Trp (RGDW) and D-Arg-Gly-Asp-Trp (D-RGDW), both of which inhibit platelet aggregation. The conformation of RGDW, and presumably that of D-RGDW, appears to be involved in its role in cellular adhesion processes. The NMR studies were interpreted as suggesting that these peptides exist as a type II′ β-turn in aqueous solution. They demonstrated that there is a high degree of conformational flexibility, but they were unable to identify any other significantly populated conformations. To increase our understanding of the structure and dynamics of these two tetrapeptides, explicit solvent molecular dynamics simulations were performed and calculated NMR observables were compared to the experimental results. Overall, good agreement was found. Analysis of the trajectories indicated that although the turn conformation is present in solution, an extended conformation is also present with a significant population. Continuum dielectric (Poisson−Boltzmann) calculations suggest that the equilibrium constant of the turn conformer and extended conformer is near unity. When comparing pK_a values calculated using the continuum dielectric models to the experimentally determined pK_a values, better agreement with experiment was found for the extended conformation than for the turn conformation. The simulations show that certain extended conformations exist in solution and that they are nearly indistinguishable from the β-turn conformation with respect to the the experimental NMR results. Using the simulation results, the best fit to all the experimental data was from a mixture of the turn and the extended conformations. Moreover, the extended conformations were found to have conformational features in common with biologically active cyclic peptides. The present analysis demonstrates that molecular dynamics simulations combined with NMR experiments provide a more complete understanding of the structure of the RGDW peptide in solution than either method alone.

Acknowledgment. We acknowledge helpful discussions with Dr. Christian Bartels, Dr. Bruno Kieffer, Dr. Patrice Koehl, and Dr. Georges Mer. We thank Dr. Michael Schaefer for his assistance with the continuum dielectric calculations. This work was supported in part by the National Science Foundation (USA), the Fondation pour la Recherche Médicale (France), and the European Economic Community (Human Capital and Mobility). The Institut de Développement et des Ressources en Informatique Scientifique (IDRIS) provided an allocation of CRAY computer time which was used for this work.

Supporting Information Available: Tables of dihedral angles and their fluctuations for the D-RGDW RDGW simulations, as well as a table of clusters obtained from the dihedral angle clustering of these simulations. Supporting Information is available free of charge via the Internet at http://pubs.acs.org.

References and Notes

(1) Ruoslahti, E.; Pierschbacher, M. D. *Cell* **1986**, *44*, 517−518.
(2) Pierschbacher, M. D.; Ruoslahti, E. *Nature* **1984**, *309*, 30−33.
(3) Yamada, K. M.; Kennedy, D. W. *J. Cell Biol.* **1984**, *99*, 29−36.
(4) Hayman, E. G.; Pierschbacker, M. D.; Ruoslahti, E. *J. Cell Biol.* **1985**, *100*, 1948−1954.
(5) Pierschbacher, M. D.; Ruolahti, E. *Proc. Natl. Acad. Sci. U.S.A.* **1984**, *81*, 5985−5988.
(6) Müller, G.; Gurrath, M.; Kessler, H. *J. Comput. Aided Mol. Des.* **1994**, *8*, 709−730.
(7) Wistow, G.; Turnell, B.; Summers, L.; Slingsby, C.; Moss, D.; Miller, L.; Lindley, P.; Blundell, T. *J. Mol. Biol.* **1983**, *170*, 175−202.
(8) Leahy, D. J.; Ikramuddin, A.; Erickson, H. P. *Cell* **1996**, *84*, 155−164.
(9) Copié, V.; Tomita, Y.; Akiyama, S. K.; Aota, S.-i.; Yamada, K. M.; Venable, R. M.; Pastor, R. W.; Krueger, S.; Torchia, D. A. *J. Mol. Biol.* **1998**, *277*, 663−682.
(10) Adler, M.; Lazarus, R. A.; Dennis, M. S.; Wagner, G. *Science* **1991**, *253*, 445−448.
(11) Saudek, V.; Atkinson, R. A.; Pelton, J. T. *Biochemistry* **1991**, *30*, 7369−7372.
(12) Cooke, A. M.; Carter, B. G.; Martin, D. M. A.; Murray-Rust, P.; Weir, M. *P. Eur. J. Biochem.* **1991**, *202*, 323−328.
(13) Gould, R. M.; Polokoft, M. A.; Friedman, P. A.; Huang, T. F.; Holt, J. T.; Cook, J. J.; Niewiarowski, S. *Proc. Soc. Exp. Biol. Med.* **1990**, *195*, 168−171.
(14) Krezel, A. M.; Wagner, G.; Seymour-Ulmer, J.; Lazarus, R. A. *Science* **1994**, *264*, 1944−1947.
(15) Logan, D.; Abu-Ghazaleh, R.; Blakemore, W.; Curry, S.; Jackson, T.; King, A.; Lea, S.; Lewis, R.; Newman, J.; Parry, N.; Rowlands, S. D.; Stuart, D.; Fry, E. *Nature* **1993**, *362*, 566−568.
(16) Grimes, J.; Basak, A. K.; Roy, P.; Stuart, D. *Nature* **1995**, *373*, 167−170.
(17) Reed, J.; Hull, W. E.; von der Lieth, C.-W.; Kübler, D.; Suhai, S.; Kinzel, V. *Eur. J. Biochem.* **1988**, *178*, 141−154.
(18) Genest, M.; Marion, D.; Ptak, M. *Second Forum on Peptides*; John Libbey Eurotext Ltd.: London, 1989; pp 415−418.
(19) Williamson, M. P.; Davies, J. S; Thomas, W. A. *J. Chem. Soc., Perkin Trans.* **1991**, *2*, 601−606.
(20) Mickos, H.; Bahr, J.; Lüning, B. *Acta Chim. Scand* **1990**, *44*, 161−164.
(21) Cachau, R. E.; Serpersu, E. H.; Mildvan, A. S.; August, J. T.; Amzel, L. M. *J. Mol. Recognit.* **1989**, *2*, 179−186.
(22) Johnson, C. W. J.; Pagano, T. G.; Basson, C. T.; Madri, J. A.; Gooley, P.; Armitage, I. M. *Biochemistry* **1993**, *32*, 268−273.
(23) Kieffer, B.; Mer, G.; Mann, A.; Lefèvre, J. F. *Int. J. Pept. Protein Res.* **1994**, *44*, 70−79.
(24) McDowell, R. S.; Gadek, T. R. *J. Am. Chem. Soc.* **1992**, *114*, 9245−9253.
(25) Kopple, K. D.; Baures, P. W.; Bean, J. W.; D'Ambrosio, C.; Hughes, J. L.; Peoshoff, C. E.; Eggleston, D. S. *J. Am. Chem. Soc.* **1992**, *114*, 9615−9623.
(26) Bach II, A. C.; Eyermann, C. J.; Gross, J. D.; Bower, M. J.; Harlow, R. L.; Weber, P. C.; DeGrado, W. F. *J. Am. Chem. Soc.* **1994**, *116*, 3207−3219.
(27) Wilmot, C. M.; Thornton, J. M. *J. Mol. Biol.* **1988**, *203*, 221−232.
(28) Sibanda, B. L.; Blundell, T. L.; Thornton, J. M. *J. Mol. Biol.* **1989**, *206*, 759−777.
(29) Wilmot, C. M.; Thornton, J. M. *Protein Eng.* **1990**, *3*, 479−493.
(30) Mattos, C.; Petsko, G. A; Karplus, M. *J. Mol. Biol.* **1994**, *238*, 733−747.
(31) Kieffer, B. *Etude Structurale et Dynamique de Peptides en Solution par RMN*; Université Louis Pasteur: Strasbourg, France, 1992.
(32) Jardetzki, O. *Biochim. Biophys. Acta* **1980**, *621*, 227−232.
(33) Wütrich, K. *NMR of Proteins and Nucleic Acids*; John Wiley & Sons: New York, 1986.
(34) Mierke, D. F.; Kurz, M.; Kessler, H. *J. Am. Chem. Soc.* **1994**, *116*, 1042−1049.
(35) Honig, B.; Hudson, B.; Sykes, B. D.; Karplus, M. *Proc. Natl. Acad. Sci. U.S.A.* **1971**, *68*, 1289−1293.
(36) Kessler, H.; Griesinger, C.; Lautz, J.; Müller, A.; van Gunsteren, W. F.; Berendsen, H. *J. Am. Chem. Soc.* **1988**, *110*, 3393−3396.
(37) Gilson, M. K.; Honig, B. H. *Proteins: Struct., Funct., Genet.* **1988**, *4*, 7−18.
(38) Davis, M. E.; McCammom, J. A. *Chem. Rev.* **1990**, *90*, 509−521.
(39) Lim, C.; Bashford, D.; Karplus, M. *J. Phys. Chem.* **1991**, *95*, 5610−5620.
(40) Brooks, B. R.; Bruccoleri, R. E.; Olafson, B. D.; States, D. J.; Swaminathan, S.; Karplus, M. *J. Comput. Chem.* **1983**, *4*, 187−217.
(41) MacKerell, A. D. J.; Bashford, D.; Bellott, M.; Dunbrack, R. L. J.; Evanseck, J. D.; Field, M. J.; Fischer, S.; Gao, J.; Guo, H.; Ha, S.; Joseph-McCarthy, D.; Kuchnir, L.; Kuczera, K.; Lau, F. T. K.; Mattos, C.; Michnick, S.; Ngo, T.; Nguyen, D. T.; Prodhom, B.; Reiher, W. E. I., III; Roux, B.; Schlenkrich, M.; Smith, J. C.; Stote, R.; Straub, J.; Watanabe, M.; Wiorkiewicz-Kuczera, J.; Yin, D.; Karplus, M. *J. Phys. Chem.* **1998**, *102*, 3586−3616.
(42) Brünger, A. T.; Karplus, M. *Proteins: Struct. Funct., Genet.* **1988**, *4*, 148−156.
(43) Gelin, B.; Karplus, M. *Proc. Natl. Acad. Sci. U.S.A.* **1977**, *74*, 801−805.
(44) Whitlow, M.; Teeter, M. M. *J. Am. Chem. Soc.* **1986**, *108*, 7163−7172.
(45) Stote, R. H.; Karplus, M. *Proteins*: *Struct., Funct., Genet.* **1995**, *23*, 12−31.
(46) Jorgensen, W. L.; Chandrasekhar, J.; Madura, J. D.; Impey, R. W.; Klein M. L., Jr. *J. Chem. Phys.* **1983**, *79*, 926−935.
(47) Neria, E.; Fischer, S.; Karplus, M. *J. Chem. Phys.* **1996**, *105*, 1902−1921.
(48) Ryckaert, J. P.; Ciccotti, G.; Berendsen, H. J. C. *J. Comput. Phys.* **1977**, *23*, 327−341.

(49) Karpen, M. E.; Tobias, D. J.; Brooks, C. L. I. *Biochemistry* **1993**, *32*, 412−420.
(50) Pao, Y.-H. *Adaptive Pattern Recognition and Neural Networks*; Addison-Wesley: New York, 1989.
(51) Carpenter, G. A.; Grossberg, S. *Appl. Opt.* **1987**, *26*, 4919−4930.
(52) Bashford, D.; Karplus, M. *Biochemistry* **1990**, *29*, 10219−1025.
(53) Yang, A.; Honig, B. *J. Mol. Biol.* **1993**, *231*, 459−474.
(54) Aralk, J. C.; Nicholls, A.; Sharp, K.; Honig, B. *J. Am. Chem. Soc.* **1991**, *113*, 1454.
(55) Warwicker, J.; Watson, H. C. *J. Mol. Biol.* **1982**, *157*, 671−679.
(56) Davis, M. E.; Madura, J. D.; Luty, B. A.; McCammon, J. A. *Comput. Phys. Commun.* **1991**, *62*, 187−197.
(57) Schaefer, M.; Sommer, M.; Karplus, M. *J. Phys. Chem.* **1997**, *101*, 1663−1683.
(58) Schaefer, M.; van Vlijmen, H. W. T.; Karplus, M. *Adv. Protein Chem.* **1998**, *51*, 1−57.
(59) van Vlijmen, H. W. T.; Schaefer, M.; Karplus, M. *Proteins: Struct., Funct., Genet.* **1998**, *33*, 145−158.
(60) Antosievicz, J.; McCammon, J. A.; Gilson, M. *J. Mol. Biol.* **1994**, *238*, 415.
(61) Dunbrack, R. L, Jr.; Karplus, M. *J. Mol. Biol.* **1993**, *230*, 543−574.
(62) Dunbrack, R. L., Jr.; Karplus, M. *Nat. Struct. Biol.* **1994**, *1*, 334−340.
(63) Bartels, C.; Stote, R. H.; Karplus, M. *J. Mol. Biol.* **1998**, *284*, 1641−1660.
(64) Hansmann, U. H. E.; Okamoto, Y.; Eisenmenger, F. *Chem. Phys. Lett.* **1996**, *259*, 321−330.
(65) Nakajima, N.; Nakamura, H.; Kidera, A. *J. Phys. Chem.* **1997**, *101*, 817−824.
(66) Bartels, C.; Karplus, M. *J. Phys. Chem. B* **1998**, *102*, 865−880.
(67) Ösapay, K.; Young, W. S.; Bashford, D.; Brooks, C. L., III; Case, D. A. *J. Phys. Chem.* **1996**, *100*, 2698−2705.
(68) Ösapay, K; Case, D. A. *J. Am. Chem. Soc.* **1991**, *113*, 9436−9444.
(69) Karplus, M. *J. Phys. Chem.* **1959**, *30*, 11−15.
(70) Pardi, A.; Billeter, M; Wüthrich, K. *J. Mol. Biol.* **1984**, *180*, 741−751.
(71) DeMarco, A.; Llinás, M.; Wüthrich, K. *Biopolymers* **1978**, *17*, 617−636.
(72) Landis, C; Allured, V. S. *J. Am. Chem. Soc.* **1991**, *113*, 9493−9499.
(73) Blackledge, M. J.; Brüschweiler, R.; Griesinger, C.; Schmidt, J. M.; Xu, P.; Ernst, R. R. *Biochemistry* **1993**, *32*, 10960−10974.
(74) Nikiforovich, G. V.; Prakash, O.; Gehrig, C. A.; Hruby, V. J. *J. Am. Chem. Soc.* **1993**, *115*, 3399−3406.
(75) Cicero, D. O.; Barbato, G.; Bazzo, R. *J. Am. Chem. Soc.* **1995**, *117*, 1027−1033.
(76) Lawson, C. L.; Hanson, R. J. *Solving Least Squares Problems*; Prentice-Hall: Englewood Cliffs, NJ, 1995.
(77) Koradi, R.; Billeter, M.; Wüthrich, K. *J. Mol. Graphics* **1996**, *14*, 51−55.